Journal of
Synchrotron
Radiation

ISSN 1600-5775

Received 22 July 2013
Accepted 14 November 2013

Studying the surface reaction between NiO and Al_2O_3 *via* total reflection EXAFS (ReflEXAFS)

Tommaso Costanzo,[a] Federico Benzi,[b] Paolo Ghigna,[a] Sonia Pin,[c] Giorgio Spinolo[a] and Francesco d'Acapito[d]*

[a]INSTM and Department of Chemistry, University of Pavia, I27100 Pavia, Italy, [b]School of Science and Technology, Geology Division, University of Camerino, I-62032 Camerino, Italy, [c]General Energy Research (ENE), Laboratory for Bioenergy and Catalysis, Paul Scherrer Institut, 5232 Villigen PSI, Switzerland, and [d]CNR-IOM-OGG, c/o ESRF, GILDA-CRG, BP 220, F-38043 Grenoble Cedex, France. *E-mail: dacapito@esrf.fr

The reaction between NiO and (0001)- and $(1\bar{1}02)$-oriented Al_2O_3 single crystals has been investigated on model experimental systems by using the ReflEXAFS technique. Depth-sensitive information is obtained by collecting data above and below the critical angle for total reflection. A systematic protocol for data analysis, based on the recently developed *CARD* code, was implemented, and a detailed description of the reactive systems was obtained. In particular, for $(1\bar{1}02)$-oriented Al_2O_3, the reaction with NiO is almost complete after heating for 6 h at 1273 K, and an almost uniform layer of spinel is found below a mixed (NiO + spinel) layer at the very upmost part of the sample. In the case of the (0001)-oriented Al_2O_3, for the same temperature and heating time, the reaction shows a lower advancement degree and a residual fraction of at least 30% NiO is detected in the ReflEXAFS spectra.

Keywords: topochemistry; spinel-forming reactions; epitaxy; non-equilibrium compounds; ReflEXAFS.

1. Introduction

Extended X-ray absorption fine-structure spectroscopy (EXAFS) is a well established method of determining the local atomic environment of a selected element in a wide variety of samples. *Per se*, EXAFS is a bulk technique. Surface sensitivity, however, can be achieved by recording the intensity of the reflected beam from a flat surface. In this detection mode the technique is called reflection EXAFS, or ReflEXAFS (Barchewitz *et al.*, 1978). One of the peculiar features of ReflEXAFS is that the depth at which the sample is being probed can be controlled by varying the incidence angle of the impinging beam (d'Acapito *et al.*, 2007). Below the critical angle (total reflection regime), the probing beam is confined as an evanescent wave in a layer just a few nanometres below the surface (Parratt, 1954). Increasing the incidence angle above the critical value, the probed depth increases sharply. However, until recently, the technique has been used mostly under the total reflection regime due to severe difficulties in data collection and analysis. Applications to buried interfaces can be retrieved in the literature, but up to now ReflEXAFS has been applied mostly to model systems. The aim of this paper is to foster the ReflEXAFS technique as a powerful tool for investigating real systems, where the structure of a thin epilayer can change with depth. In particular, attention has been focused on the chemical reactivity in the solid state at the nano-scale, having in mind, in particular, oxide systems. At the length scale of micrometres or above, the growth of a product phase is diffusion-controlled, a well established topic of the scientific literature [the basic approach (Wagner, 1936; Schmalzried, 1981, 1995) as well as more recent studies on kinetics and mechanisms of the reactivity in technologically important oxide systems such as superconductors or fuel cells components (Flor *et al.*, 1990, 1995; Anselmi-Tamburini *et al.*, 1991; Spinolo *et al.*, 1992, 1993; Ghigna *et al.*, 1993; Faaland *et al.*, 1999; Lahl *et al.*, 2002; Buscaglia *et al.*, 2002; Yang & Wei, 2004; Jancar *et al.*, 2004; Yuw & Fung, 2006; Dahl *et al.*, 2007; Tolchard & Grande, 2007*a*,*b*; Palcut *et al.*, 2007*a*,*b*; Waernhus *et al.*, 2007; Kishimoto *et al.*, 2007; Backhaus-Ricoult, 2008; Peiteado *et al.*, 2008; Bernardo *et al.*, 2011)]. At the nano-scale the control of a heterogeneous chemical reaction is taken by the jumps of atoms or ions across one or the other interface between product and reagents and the growth typically follows a linear time law. The most popular model oxide system investigated in this regard is the NiO + Al_2O_3 system leading to the Ni–Al spinel ($NiAl_2O_4$). As a matter of fact, the chemical reactivity at this level of analysis is associated with phenomena such as epitaxy and its evolution in time, strain build-up, misfit accommodation, de-wetting, volume expansion, lattice rotations, and generally with complex texture evolution and strong dependence from interfacial free enthalpy (Hesse *et al.*, 1994;

Hesse, 1997; Bench *et al.*, 1997; Kotula & Carter, 1998*a*,*b*; Kotula *et al.*, 1998; Johnson & Carter, 1998; Hesse & Senz, 2004; Graff *et al.*, 2005; Farrer & Carter, 2006; Lotnyk *et al.*, 2008; Altay *et al.*, 2009; Arredondo *et al.*, 2009; Basu *et al.*, 2011). Strongly related to these aspects is the more recent use of heterogeneous reactions between nano-sized solid reagents to produce appealing nano-structures (Yin *et al.*, 2004; Fan *et al.*, 2006, 2007; Yang *et al.*, 2008*a*,*b*; Qiu & Yang, 2008; Cabot *et al.*, 2009*a*,*b*; Peng *et al.*, 2009). Finally, going to the very early times and to the smallest length scales of a heterogeneous reaction, interest becomes focused on the processes that control nucleation, *i.e.* the formation of a product phase in between two grains of the reagents. This is in a sense the true chemical reaction and has been much less investigated with respect to the other reaction regimes (Kotula & Carter, 1995). Concerning the last topic, we have recently shown (Ghigna *et al.*, 2003, 2010, 2011; d'Acapito *et al.*, 2003*a*,*b*; Pin *et al.*, 2009, 2011, 2013*a*,*b*) the effectiveness of an approach to the chemical reactivity in the solid state based on the use of model reacting systems ($NiO + Al_2O_3$ and particularly $ZnO + Al_2O_3$) made of a thin layer of one reagent deposited onto a single-crystal slab of the other reagent. The system is investigated by combining several experimental techniques and comparing the results obtained starting from different film-to-crystal orientations and different film thicknesses. The reaction can be quenched at different advancement degrees; the sample is allowed to react partially thus forming an epi-layer where both composition and crystal structure change with time and depth. The use of ReflEXAFS appears to be very promising in this regard, in particular due to its capability to investigate buried interfaces and multilayer systems (Heald *et al.*, 1988), and to retrieve local structural parameters from layered systems. The reflectivity $\mathcal{R}$ is a complex function of photon energy E as it depends on both the imaginary and real parts of the sample optical constants. Features analogous to the EXAFS oscillations are still visible above the absorption edge, but their analysis is considerably more complex. Quantitative rigorous methods for analyzing this class of data have been proposed in the past years (Heald *et al.*, 1988; Borthen & Strehblow, 1997; Benzi *et al.*, 2008; López-Flores *et al.*, 2009) but have been used only in a restricted number of cases. In the past, our group has already used ReflEXAFS to study the initial steps of reactions in the solid state (d'Acapito *et al.*, 2003*a*; Ghigna *et al.*, 2003). The present contribution uses the *CARD* code (http://www.esrf.fr/computing/scientific/CARD/CARD.html), which is based on the method presented by Benzi *et al.* (2008) and has been recently extended to the case of layered systems.

2. Experimental

2.1. Sample preparation

Thin films of NiO (25 nm thick) have been deposited onto $(1\bar{1}02)$- and (0001)-oriented Al_2O_3 single crystals using RF magnetron sputtering and starting from Cerac (99.995%) NiO. The deposition details have been reported elsewhere (Pin *et al.*, 2009). An as-deposited NiO film, without any thermal treatment, was used as a reference for pure NiO (hereafter sample 1). The other deposited films have been fired at 1273 K for 6 h. For the $(1\bar{1}02)$-oriented single-crystal substrate (sample 2), the reaction yielding the $NiAl_2O_4$ spinel appears as almost complete. The chemical reaction proceeds also for the film deposited onto the other interface (sample 3), but with only a partial conversion of NiO to spinel.

2.2. ReflEXAFS data collection and analysis

ReflEXAFS data at the Ni *K*-edge ($E = 8333$ eV) have been collected at the GILDA beamline (d'Acapito *et al.*, 1998) operative at the European Synchrotron Radiation Facility on a dedicated experimental station (d'Acapito *et al.*, 2003*b*). The monochromator was equipped with a pair of Si (311) crystals and was used in dynamical focusing mode. A pair of Pd-coated mirrors ($E_{\rm cutoff} \simeq 18$ keV) was used for harmonic rejection and for the vertical focus on the sample. The incident and reflected beams have been collected by two ion chambers, and a preliminary spectrum without the sample was used to scale the reflected intensity to absolute reflectivity values. The primary beam was shaped by a slit to 50 µm and in all the measurements it was ensured that the footprint of the beam was shorter than the sample.

For each sample, reflectivity curves at fixed energy E and variable angle φ, $\mathcal{R}^E(\varphi)$, were first collected at $E = 8100$ eV, 8400 eV and 9000 eV; these correspond to points *before*, *just after* and *far after* the edge, respectively.

From $\mathcal{R}^E(\varphi)$ two angles were selected for the ReflEXAFS data collection: one before and one just after the critical angle for total reflection. The actual values were $\varphi = 0.2^\circ$ and 0.32°. This realises the desired depth-sensitive measurement, the lower-angle spectrum accounting for the surface and the higher-angle spectrum accounting for the deeper part of the sample.

As already noted, the data analysis was carried out using the *CARD* code. The overall procedure can be summarized as follows: as a first step, *CARD* fits the reflectivity $\mathcal{R}^E(\varphi)$ to assess a model for the set of layers constituting the sample. In addition to thickness, electron density and roughness of each layer, the fitting model also accounts for instrument-related parameters, such as error in the absolute angular determination, overall normalization and background. This information is then used (*a*) to generate the theoretical ReflEXAFS spectra $\mathcal{R}^\varphi(E)$ at the selected angles φ and (*b*) to calculate modified theoretical EXAFS paths to fit the oscillating part of each $\mathcal{R}^\varphi(E)$. A more thorough description of the working principle of *CARD* can be found in Benzi *et al.* (2008). It is worth noting that in the formalism used here the ReflEXAFS signal χ_R is defined as $\mathcal{R} - \mathcal{R}_{\rm atomic}$. This simple choice permits data collected either at low angle (where the edge appears with a downwards step) and at high angle (where the edge no longer possesses a step-like shape) to be treated in a coherent way. Care should be taken as the resulting χ_R spectrum appears to be reversed when compared with the standard χ_μ data (which come from spectra with an upwards step).

Table 1
Fitting results of reflectivity data for sample 1 collected at 8100 eV.

Data are shown in Fig. 1.

Layer	Parameter	
Substrate	Roughness (Å)	9.3 (9)
NiO	Thickness (Å)	253 (25)
NiO	Roughness (Å)	38 (4)
NiO	Density (g cm^{-3})	6.7 (7)

3. Results and discussion

Sample 1 is the pure unreacted NiO; here it is modelled as a NiO layer on an Al_2O_3 substrate. For this sample, Table 1 summarizes the fitting parameters of the reflectivity curve $\mathcal{R}^{8100}(\varphi)$, whereas Fig. 1 shows the experimental data with the best fit. The thickness of the NiO layer obtained from the fit is in good agreement with the value (250 Å) determined with a quartz microbalance during the deposition process, and the density compares well with the literature value (6.67 g cm^{-3}). The slight misfit at low angles is probably due to a more complex layer structure of the sample near the surface but attempts to cure it did not lead to significant improvements. On the other hand, we have verified (as also done for the other samples) that the results of the fits at the other two energy values were in good agreement with the above data.

The $\mathcal{R}^{0.2}(E)$ spectrum has then been modelled as shown in Fig. 2(*a*). From the parameters relative to the sample (thickness, density, *etc.*), modified EXAFS paths (Benzi *et al.*, 2008) have been generated starting from those calculated for NiO with the *Feff8.1* code (Ankudinov *et al.*, 1998). The ReflEXAFS data $\chi_R(k)$, here defined as $\mathcal{R}(E) - \mathcal{R}_{\rm atomic}(E)$, have been extracted using the *ATHENA* code (Ravel & Newville, 2005) from the raw data, and then fitted using the *ARTEMIS* code (Ravel & Newville, 2005) with the modified EXAFS paths.

The ReflEXAFS spectrum is shown in Fig. 3 and at a qualitative level it closely follows the spectrum of the NiO powder. Modelling was carried out using only the first two shells (Ni–O and Ni–Ni) of the NiO local structure. The fit was carried out in *r* space (Fourier transforms, in Fig. 4) using a k^2-weighting factor; the parameter values are shown in Table 2, and the comparison between data and fit is shown in Figs. 3 and 4. The experiment is well reproduced by the fit, and the Ni–O and Ni–Ni distances retrieved by the fit are in excellent agreement with the crystallographic data.

Sample 2 is the NiO layer deposited on the $(1\bar{1}02)$ face and annealed for 6 h at 1273 K; Fig. 3 shows the experimental ReflEXAFS data along with those of the $NiAl_2O_4$ and NiO powder standards. For both incidence angles the spectra of this

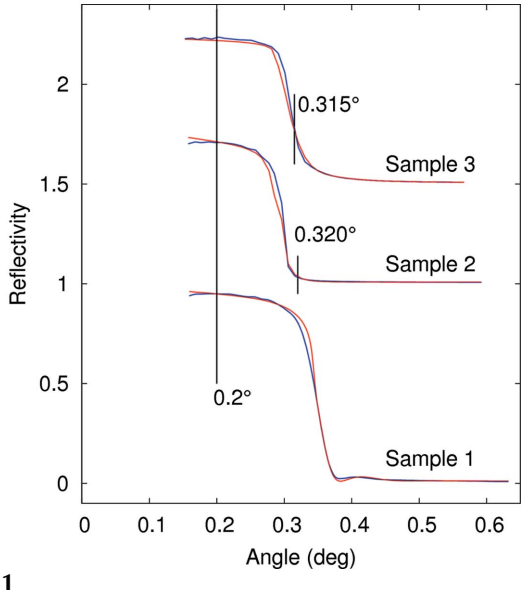

Figure 1
Reflectivity $\mathcal{R}^E(\varphi)$ at 8100 eV for samples 1, 2 and 3. Blue line: experimental; red line: best fit. The vertical lines mark the collection angles used for the ReflEXAFS data.

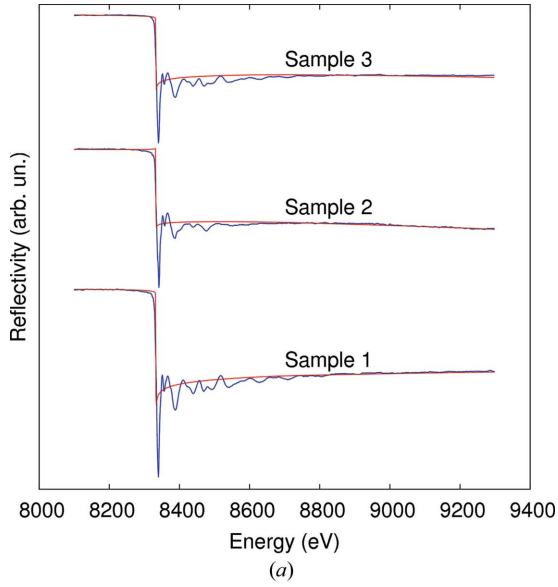

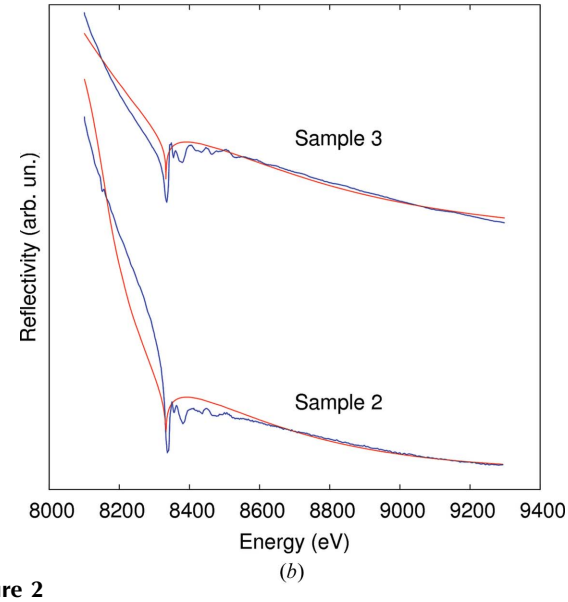

Figure 2
(*a*) $\mathcal{R}^{\varphi}(E)$ for samples 1, 2 and 3 collected at 0.2°. Colours are as in Fig. 1. (*b*) $\mathcal{R}^{\varphi}(E)$ for samples 2 and 3 collected at the highest angle. Colours are as in Fig. 1.

Table 2
Summary of the parameters for the EXAFS fitting of sample 1.

Coordination numbers are the same as in the crystal structure. Errors are given in parentheses. If the error is not shown, the parameter was kept fixed to the theoretical value in the fitting.

Parameter	Theoretical	Result
E_0 (eV)		−7(2)
r Ni–O (Å)	2.097	2.09 (4)
r Ni–Ni (Å)	2.966	2.97 (2)
σ^2 Ni–O (Å^2)	–	0.009 (4)
σ^2 Ni–Ni (Å^2)	–	0.007 (1)

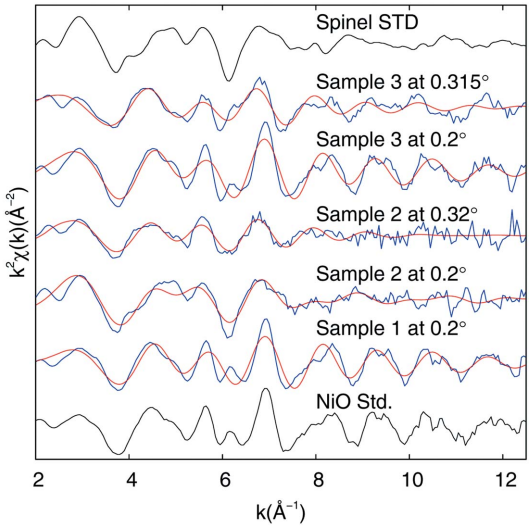

Figure 3
ReflEXAFS spectra (blue line) with the best fit (red) collected at 0.2° and at high angle (0.32° or 0.315°) for samples 1, 2 and 3. In order to present signals with comparable amplitudes the spectra in total reflection of samples 2 and 3 were multiplied by a factor of two and those at high angles by a factor of four. The spectra of the model compounds (NiO and $NiAl_2O_4$) taken in transmission mode are multiplied by −1.

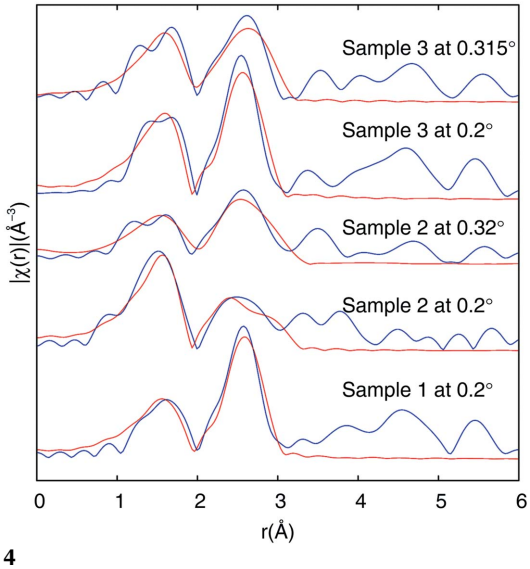

Figure 4
Fourier transforms of the ReflEXAFS spectra (blue line) with the best fit (red) collected at 0.2° and at high angle (0.32° or 0.315°) for samples 1, 2 and 3. The multiplication factors are the same as in Fig. 3.

Table 3
Fitting results of reflectivity data for sample 2 collected at 8100 eV.

Errors are given in parentheses. If the error is not shown, the parameter was kept fixed to the theoretical value in the fitting. Data are shown in Fig. 1.

Sample layer	Parameter	
Substrate	Roughness (Å)	59 (6)
NiO/$NiAl_2O_4$ 10/90	Thickness (Å)	64 (6)
NiO/$NiAl_2O_4$ 10/90	Roughness (Å)	46 (5)
NiO/$NiAl_2O_4$ 10/90	Density (g cm^{-3})	4.7 (5)
$NiAl_2O_4$	Thickness (Å)	179 (18)
$NiAl_2O_4$	Roughness (Å)	59 (6)
$NiAl_2O_4$	Density (g cm^{-3})	4.4

Table 4
EXAFS fit results of sample 2 at 0.203° and 0.320°.

Errors are given in parentheses. If the error is not shown, the parameter was kept fixed to the theoretical value in the fitting.

	Data at 0.203°		Data at 0.320°
Parameter	Theoretical	Result	Result
NiO			
r Ni–O (Å)	2.097	2.097	
r Ni–Ni (Å)	2.966	3.01 (5)	
$NiAl_2O_4$			
r Ni–O (Å)	1.969	2.06 (2)	2.06 (2)
r Ni–Ni (Å)	2.844	2.83 (4)	3.00 (6)
r Ni–Al (Å)	2.844	2.8 (2)	2.80 (2)
r Ni–Al (Å)	3.335	3.3 (2)	3.28 (3)
For every structure			
E_0 (eV)		−6 (2)	3 (2)
σ^2 Ni–O (Å^2)	–	0.0073	0.016 (4)
σ^2 Ni–Ni, Ni–Al (Å^2)	–	0.0047	0.004 (1)
$NiAl_2O_4$/NiO (%)	90	88 (6)	

sample are strongly similar to that of $NiAl_2O_4$, a clear indication of the onset of the chemical reaction leading to $NiAl_2O_4$ and triggered by the thermal treatment. Accordingly, the layer structure of this sample is then modelled with (*a*) substrate, (*b*) a buried layer (spinel) and (*c*) a surface layer mixture of NiO and $NiAl_2O_4$. With this model the $\mathcal{R}^{8100}(\varphi)$ spectrum is fitted as shown in Fig. 1, while the parameters are presented in Table 3. The density of the $NiAl_2O_4$ layer has been kept fixed in the fit to its theoretical value (4.4 g cm^{-3}), while the density of the surface layer has been left free to change. A value of 4.7 g cm^{-2} has been found corresponding to a NiO and $NiAl_2O_4$ mixture with the ratio 10/90. $\mathcal{R}(E)$ data have been collected at 0.203° and at 0.320° and are shown in Fig. 2 along with their fits. ReflEXAFS data at both angles and the related best-fitting curves are shown in Figs. 3 and 4. For $NiAl_2O_4$, a (completely) inverse spinel structure has been used and a Ni–O shell, a Ni–Ni shell and two Ni–Al shells have been considered. The structural results from the ReflEXAFS data collected at 0.203° are shown in Table 4. Here, the advancement degree is 88%, in agreement with the reflectivity data and meaning that the reaction can be considered as complete. Note that, in order to obtain more stable fits, the σ^2 values have been fixed to those of the powder $NiAl_2O_4$ model compound taken in transmission mode. For data collected at

Table 5
Fitting results of reflectivity data for sample 3 collected at 8100 eV.

Errors are given in parentheses. If the error is not shown, the parameter was kept fixed to the theoretical value in the fitting. Data are shown in Fig. 1.

Layer	Parameter	
Substrate	Roughness (Å)	29 (3)
$NiO/NiAl_2O_4$ 30/70	Thickness (Å)	169 (16)
$NiO/NiAl_2O_4$ 30/70	Roughness (Å)	15 (1)
$NiO/NiAl_2O_4$ 30/70	Density (g cm^{-3})	4.7 (5)
$NiAl_2O_4$	Thickness (Å)	82 (8)
$NiAl_2O_4$	Roughness (Å)	30 (3)
$NiAl_2O_4$	Density (g cm^{-3})	4.4 (4)

0.320° the fit model is a pure spinel layer; this is explained considering that, by increasing the incidence angle and the thickness of the probed layer, the surface NiO layer becomes negligible. A noteworthy result is that the parameters retrieved by the fit differ from those of bulk $NiAl_2O_4$, especially for what concerns the second (Ni–Ni) shell. Presumably, this indicates that at the reactive interface (the part of sample that ReflEXAFS can probe at this angle) the spinel structure is somewhat distorted, with some Ni in the tetrahedral sites or in the free octahedral sites of the spinel structure.

Sample 3 is the NiO layer deposited on the (0001) face and thermally treated as sample 2. The overall layer model is here the same as for the previous sample. Fig. 1 shows the $\mathcal{R}^{8100}(\varphi)$ spectrum and Table 5 the parameters retrieved from the reflectivity fit whereas Fig. 2 shows the $\mathcal{R}^{\varphi}(E)$ spectra. The fit of the reflectivity data now gives a surface layer containing 30% NiO and 70% $NiAl_2O_4$ above a pure spinel layer. When compared with the previous sample [NiO deposited onto the $(1\bar{1}02)$ single-crystal face], the fit clearly shows lower reactivity, as well as lower 'roughness' and higher 'thickness' of the surface layer. Moreover, as carried out for the other samples, these parameters have been used to fit the $\mathcal{R}$ *versus* E spectra. The ReflEXAFS spectra (Figs. 3 and 4) exhibit a qualitative similarity to that of powder NiO at low φ, and a hybrid character at higher φ. The parameters retrieved from the fit are reported in Table 6 and confirm the qualitative data with only a 45% spinel content in the surface to be compared with the 88% found in sample 2 that confirms the lower reactivity of the (0001) face with respect to $(1\bar{1}02)$.

4. Conclusion

In this work we have investigated the reaction in the solid state between NiO and Al_2O_3 using the ReflEXAFS technique on a model experimental system made of a thin NiO layer deposited onto two different orientations of single-crystal alumina substrates and allowed to react at 1273 K for 6 h. The *CARD* code in its new release permitted the analysis of layered samples.

It is shown that depth-sensitive information is obtained by collecting data above and below the critical angle for total reflection, thus probing (*a*) a surface layer a few tens of angströms thick or (*b*) a larger depth of the investigated sample. For the $(1\bar{1}02)$ substrate orientation, the reaction with

Table 6
EXAFS fit results for sample 3 at 0.203° and 0.315°.

Errors are given in parentheses. If the error is not shown, the parameter was kept fixed to the theoretical value in the fitting.

	Data at 0.203°		Data at 0.315°
Parameter	Theoretical	Result	Result
NiO			
r Ni–O (Å)	2.097	2.097	2.097
r Ni-Ni (Å)	2.966	3.01 (5)	2.98 (3)
$NiAl_2O_4$			
r Ni–O (Å)	1.969	2.06 (4)	2.05 (2)
r Ni–Ni (Å)	2.844	2.84	2.84
r Ni–Al (Å)	2.844	2.81 (4)	2.8 (1)
r Ni–Al (Å)	3.335	3.30 (5)	3.2 (1)
For every structure			
E_0 (eV)		−5 (2)	−1 (3)
σ^2 Ni–O (Å^2)		0.0073	0.0073
σ^2 Ni–Ni, Ni–Al (Å^2)		0.0047	0.0047
$NiAl_2O_4$/NiO (%)	70	45 (8)	61 (14)

NiO upon annealing at 1273 K is almost complete and an almost uniform layer of spinel is found below a mixed (NiO + spinel) layer at the very upmost part of the sample. A remarkable capability of the technique is that it also provides evidence of some structural distortion of the buried layer with respect to the pertinent standard phase. In the case of the (0001) substrate orientation, the reaction shows a lower advancement degree with a residual fraction of at least 30% NiO.

ESRF is acknowledged for provision of beam time (experiments CH-3151). This paper is essentially based on the thesis work submitted by two of the authors (TC and SP) in fulfilment, respectively, of a 'Laurea' degree in Chemistry at Università di Pavia and of a PhD degree in Chemical Sciences at Università di Pavia and at the Université Franco–Italienne (thèse en cotutelle). TC also acknowledges the Erasmus Placement program for financial support.

References

d'Acapito, F., Colonna, S., Pascarelli, S., Antonioli, G., Balerna, A., Bazzini, A., Boscherini, F., Campolungo, F., Chini, G., Dalba, G., Davoli, I., Fornasini, P., Graziola, R., Licheri, G., Meneghini, C., Rocca, F., Sangiorgio, L., Sciarra, V., Tullio, V. & Mobilio, S. (1998). *ESRF Newsl.* **30**, 42–44.

d'Acapito, F., Davoli, I., Ghigna, P. & Mobilio, S. (2003*b*). *J. Synchrotron Rad.* **10**, 260–264.

d'Acapito, F., Ghigna, P., Alessandri, I., Cardelli, A. & Davoli, I. (2003*a*). *Nucl. Instrum. Methods Phys. Res. B*, **200**, 421–424.

d'Acapito, F., Milita, S., Satta, A. & Colombo, L. (2007). *J. Appl. Phys.* **102**, 043524.

Altay, A., Carter, C. B. & Gülgün, M. A. (2009). *J. Mater. Sci.* **44**, 84–92.

Ankudinov, A. L., Ravel, B., Rehr, J. J. & Conradson, S. D. (1998). *Phys. Rev. B*, **58**, 7565.

Anselmi-Tamburini, U., Ghigna, P., Spinolo, G. & Flor, G. (1991). *J. Phys. Chem. Solids*, **52**, 715–721.

Arredondo, M., Saunders, M., Petraru, A., Kohlstedt, H., Vrejoiu, I., Alexe, M., Hesse, D., Browning, N. D., Munroe, P. & Nagarajan, V. (2009). *J. Mater. Sci.* **44**, 5297–5306.

Backhaus-Ricoult, M. (2008). *Solid State Sci.* **10**, 670–688.

Barchewitz, R., Cremonese-Visicato, M. & Onori, G. (1978). *J. Phys. C*, **11**, 4439–4445.

Basu, J., Suresh, A., Wilhite, B. A. & Carter, C. B. (2011). *J. Eur. Ceram. Soc.* **31**, 1421–1429.

Bench, M. W., Kotula, P. G. & Carter, C. (1997). *Surf. Sci.* **391**, 183–195.

Benzi, F., Davoli, I., Rovezzi, M. & d'Acapito, F. (2008). *Rev. Sci. Instrum.* **79**, 103902.

Bernardo, M., Jardiel, T., Peiteado, M., Caballero, A. & Villegas, M. (2011). *J. Eur. Ceram. Soc.* **31**, 3047–3053.

Borthen, P. & Strehblow, H. H. (1997). *J. Phys. IV*, C**2**, 187–189.

Buscaglia, V., Buscaglia, M., Giordano, L., Martinelli, A., Viviani, M. & Bottino, C. (2002). *Solid State Ion.* **146**, 257–271.

Cabot, A., Alivisatos, A. P., Puntes, V. F., Balcells, L., Iglesias, O. & Labarta, A. (2009*a*). *Phys. Rev. B*, **79**, 094419.

Cabot, A., Ibanez, M., Guardia, P. & Alivisatos, A. P. (2009*b*). *J. Am. Chem. Soc.* **131**, 11326–11328.

Dahl, P. I., Haugsrud, R., Lein, H. L., Grande, T. & Norby, T. (2007). *J. Eur. Ceram. Soc.* **27**, 4461–4471.

Faaland, S., Einarsrud, M., Wiik, K., Grande, T. & Høier, R. (1999). *J. Mater. Sci.* **34**, 5811–5819.

Fan, H. J., Knez, M., Scholz, R., Hesse, D., Nielsch, K., Zacharias, M. & Gösele, U. (2007). *Nano Lett.* **7**, 993–997.

Farrer, J. K. & Carter, C. B. (2006). *J. Mater. Sci.* **41**, 5169–5184.

Flor, G., Ghigna, P., Anselmi-Tamburini, U. & Spinolo, G. (1995). *J. Solid State Chem.* **116**, 314–320.

Flor, G., Scavini, M., Anselmi-Tamburini, U. & Spinolo, G. (1990). *Solid State Ion.* **43**, 77–83.

Ghigna, P., Anselmi-Tamburini, U., Spinolo, G. & Flor, G. (1993). *J. Phys. Chem. Solids*, **54**, 107–116.

Ghigna, P., Pin, S., Spinolo, G., Newton, M. A., Chiara Tarantino, S. & Zema, M. (2011). *Radiat. Phys. Chem.* **80**, 1109–1111.

Ghigna, P., Pin, S., Spinolo, G., Newton, M. A., Zema, M., Tarantino, S. C., Capitani, G. & Tatti, F. (2010). *Phys. Chem. Chem. Phys.* **12**, 5547–5550.

Ghigna, P., Spinolo, G., Alessandri, I., Davoli, I. & d'Acapito, F. (2003). *Phys. Chem. Chem. Phys.* **5**, 2244–2247.

Graff, A., Senz, S., Völtzke, D., Abicht, H. & Hesse, D. (2005). *J. Eur. Ceram. Soc.* **25**, 2201–2206.

Heald, S., Chen, H. & Tranquada, J. (1988). *Phys. Rev. B*, **38**, 1016–1026.

Hesse, D. (1997). *Solid State Ion.* **95**, 1–15.

Hesse, D. & Senz, S. (2004). *Z. Metallkdd.* **95**, 252–257.

Hesse, D., Sieber, H., Werner, P., Hillebrand, R. & Heydenreich, J. (1994). *Z. Phys. Chem.* **187**, 161–178.

Jancar, B., Valant, M. & Suvorov, D. (2004). *Chem. Mater.* **16**, 1075–1082.

Jin Fan, H., Knez, M., Scholz, R., Nielsch, K., Pippel, E., Hesse, D., Zacharias, M. & Gösele, U. (2006). *Nat. Mater.* **5**, 627–631.

Johnson, M. T. & Carter, C. B. (1998). *Microsc. Microanal.* **4**, 141–145.

Kishimoto, H., Sakai, N., Horita, T., Yamaji, K., Brito, M. E. & Yokokawa, H. (2007). *Solid State Ion.* **178**, 1317–1325.

Kotula, P. G. & Carter, C. B. (1995). *J. Am. Ceram. Soc.* **78**, 248–250.

Kotula, P. & Carter, C. (1998*a*). *J. Am. Ceram. Soc.* **81**, 2877–2884.

Kotula, P. G. & Carter, C. B. (1998*b*). *J. Am. Ceram. Soc.* **81**, 2869–2876.

Kotula, P., Johnson, M. & Carter, C. (1998). *Z. Phys. Chem.* **206**, 73–99.

Lahl, N., Bahadur, D., Singh, K., Singheiser, L. & Hilpert, K. (2002). *J. Electrochem. Soc.* **149**, a607.

López-Flores, V., Ansell, S., Ramos, S., Bowron, D. T., Díaz-Moreno, S. & &Muñoz-Páez, A. (2009). *J. Phys. Conf. Ser.* **190**, 012110.

Lotnyk, A., Graff, A., Senz, S., Zakharov, N. D. & Hesse, D. (2008). *Solid State Sci.* **10**, 702–708.

Palcut, M., Wiik, K. & Grande, T. (2007*a*). *J. Phys. Chem. C*, **111**, 813–822.

Palcut, M., Wiik, K. & Grande, T. (2007*b*). *J. Phys. Chem. B*, **111**, 2299–2308.

Parratt, L. (1954). *Phys. Rev.* **95**, 359–369.

Peiteado, M., Makovec, D., Villegas, M. & Caballero, A. C. (2008). *J. Solid State Chem.* **181**, 2456–2461.

Peng, Q., Sun, X.-Y., Spagnola, J. C., Saquing, C., Khan, S. A., Spontak, R. J. & Parsons, G. N. (2009). *ACS NaNo.* **3**, 546–554.

Pin, S., Ghigna, P., Spinolo, G., Quartarone, E., Mustarelli, P., d'Acapito, F., Migliori, A. & Calestani, G. (2009). *J. Solid State Chem.* **182**, 1291–1296.

Pin, S., Newton, M. A., d'Acapito, F., Zema, M., Tarantino, S. C., Spinolo, G., De Souza, R. A., Martin, M. & Ghigna, P. (2011). *J. Phys. Chem. C*, **116**, 980–986.

Pin, S., Suardelli, M., d'Acapito, F., Spinolo, G., Zema, M., Tarantino, S. C., Barba, L. & Ghigna, P. (2013*a*). *J. Phys. Chem. C*, **117**, 6113–6119.

Pin, S., Suardelli, M., d'Acapito, F., Spinolo, G., Zema, M., Tarantino, S. C. & Ghigna, P. (2013*b*). *J. Phys. Chem. C*, **117**, 6105–6112.

Qiu, Y. & Yang, S. (2008). *Nanotechnology*, **19.**

Ravel, B. & Newville, M. (2005). *J. Synchrotron Rad.* **12**, 537–541.

Schmalzried, H. (1981). *Solid State Reactions.* Weinheim: Verlag Chemie.

Schmalzried, H. (1995). *Chemical Kinetics of Solids.* Weinheim: Wiley-VCH.

Spinolo, G., Anselmi-Tamburini, U., Ghigna, P., Chiodelli, G. & Flor, G. (1992). *J. Phys. Chem. Solids*, **53**, 591–599.

Spinolo, G., Anselmi-Tamburini, U., Ghigna, P. & Flor, G. (1993). *Physica C*, **217**, 347–359.

Tolchard, J. & Grande, T. (2007*a*). *J. Solid State Chem.* **180**, 2808–2815.

Tolchard, J. R. & Grande, T. (2007*b*). *Solid State Ion.* **178**, 593–599.

Waernhus, I., Sakai, N., Yokokawa, H., Grande, T., Einarsrud, M.-A. & Wiik, K. (2007). *Solid State Ion.* **178**, 907–914.

Wagner, C. (1936). *Z. Phys. Chem. B*, **34**, 309.

Yang, C. & Wei, W. (2004). *J. Am. Ceram. Soc.* **87**, 1110–1116.

Yang, Y., Kim, D. S., Knez, M., Scholz, R., Berger, A., Pippel, E., Hesse, D., Gosele, U. & Zacharias, M. (2008*a*). *J. Phys. Chem. C*, **112**, 4068–4074.

Yang, Y., Kim, D. S., Scholz, R., Knez, M., Lee, S. M., Gosele, U. & Zacharias, M. (2008*b*). *Chem. Mater.* **20**, 3487–3494.

Yin, Y. D., Rioux, R. M., Erdonmez, C. K., Hughes, S., Somorjai, G. A. & Alivisatos, A. P. (2004). *Science*, **304**, 711–714.

Yuw, H.-C. & Fung, K.-Z. (2006). *J. Am. Ceram. Soc.* **89**, 2881–2886.